Sieve element occlusion (*SEO*) genes encode structural phloem proteins involved in wound sealing of the phloem

Antonia M. Ernst[a], Stephan B. Jekat[a], Sascia Zielonka[a], Boje Müller[a], Ulla Neumann[b], Boris Rüping[c], Richard M. Twyman[d], Vladislav Krzyzanek[e,f], Dirk Prüfer[a,c,1], and Gundula A. Noll[c]

[a]Fraunhofer Institute for Molecular Biology and Applied Ecology, 48143 Münster, Germany; [b]Max Planck Institute for Plant Breeding Research, 50829 Cologne, Germany; [c]Institute of Plant Biology and Biotechnology, University of Muenster, 48143 Münster, Germany; [d]Department of Biology, University of Warwick, Coventry CV4 7AL, United Kingdom; [e]Institute of Medical Physics and Biophysics, University of Muenster, 48149 Münster, Germany; and [f]Institute of Scientific Instruments, Academy of Sciences of the Czech Republic, 61264 Brno, Czech Republic

Edited* by Patricia C. Zambryski, University of California, Berkeley, CA, and approved May 28, 2012 (received for review February 23, 2012)

The *sieve element occlusion* (*SEO*) gene family originally was delimited to genes encoding structural components of forisomes, which are specialized crystalloid phloem proteins found solely in the Fabaceae. More recently, *SEO* genes discovered in various non-Fabaceae plants were proposed to encode the common phloem proteins (P-proteins) that plug sieve plates after wounding. We carried out a comprehensive characterization of two tobacco (*Nicotiana tabacum*) *SEO* genes (*NtSEO*). Reporter genes controlled by the *NtSEO* promoters were expressed specifically in immature sieve elements, and GFP-SEO fusion proteins formed parietal agglomerates in intact sieve elements as well as sieve plate plugs after wounding. NtSEO proteins with and without fluorescent protein tags formed agglomerates similar in structure to native P-protein bodies when transiently coexpressed in *Nicotiana benthamiana*, and the analysis of these protein complexes by electron microscopy revealed ultrastructural features resembling those of native P-proteins. *NtSEO*-RNA interference lines were essentially devoid of P-protein structures and lost photoassimilates more rapidly after injury than control plants, thus confirming the role of P-proteins in sieve tube sealing. We therefore provide direct evidence that *SEO* genes in tobacco encode P-protein subunits that affect translocation. We also found that peptides recently identified in fascicular phloem P-protein plugs from squash (*Cucurbita maxima*) represent cucurbit members of the SEO family. Our results therefore suggest a common evolutionary origin for P-proteins found in the sieve elements of all dicotyledonous plants and demonstrate the exceptional status of extrafascicular P-proteins in cucurbits.

photoassimilate transport | wound response | exudation | phloem protein 1

The sieve elements of most angiosperms contain P-proteins, i.e., specialized structural proteins thought to facilitate rapid wound sealing after injury to prevent the loss of turgor and photosynthate (1, 2). P-proteins have been identified in all dicotyledonous plants studied thus far and also in some monocotyledonous plants, with palms and grasses as the main exceptions (3).

In higher plants, the photosynthate is transported in sieve tubes composed of consecutively arranged sieve elements. Sieve elements are connected to each other through converted plasmodesmata, forming sieve pores that facilitate translocation (4). The synthesis of P-proteins begins in immature, nucleated sieve elements (5), resulting in electron-dense proteinaceous structures. Their ultrastructural characteristics have been described variously as granular, fibrillar, or tubular, even within the same cell (6–14), and today these structures are thought to represent the various different stages of P-protein differentiation (3). In young sieve elements, subunits accumulate within the cytoplasm, forming large P-protein bodies (9). Toward the end of sieve element maturation, selective autolysis results in the degradation of the tonoplast, nucleus, and other organelles, whereupon the P-protein bodies disperse into smaller aggregates that move to the periphery of the cell, remaining in this position in the mature, functional sieve tubes (1). There has been much speculation about the function of P-proteins (15), but substantial evidence points toward having a role in rapid phloem wound sealing (2, 16). Following injury, conventional P-proteins detach from their parietal position and form plugs at sieve plates to block further translocation (1). Indeed, the pores of damaged sieve tubes become entirely filled with proteinaceous fibrillar material (17).

Despite the wealth of structural and functional data, little is known about P-proteins at the molecular level. The first structural P-protein to be characterized was phloem protein 1 (PP1) from squash (*Cucurbita maxima*) (18). This filament protein was immunolocalized in sieve element slime plugs and P-protein bodies, whereas the corresponding mRNA was shown to accumulate in companion cells (19). PP1 also was shown to be translocated within the extraordinary extrafascicular phloem system of Cucurbitaceae (20). However, the fact that PP1 is potentially unique to cucurbit species (21), whereas the typical P-protein structures in fascicular sieve elements are morphologically comparable in all dicotyledonous angiosperms, is still a matter of debate. Recently, the isolation and sequencing of the plug-forming proteins from squash fascicular sieve tubes resulted in the identification of proteins apparently unrelated to PP1, whereas PP1 was found to be associated with the extrafascicular phloem system (22). The identity of the typical P-protein structures found in the fascicular phloem of *C. maxima* and all dicotyledonous plants therefore has remained elusive.

Thus far, four *sieve element occlusion* (*SEO*) gene family members have been identified in *Medicago truncatula* (*MtSEO-F1–F4*) and *Glycine max* (*GmSEO-F1–F4*) and characterized as encoding forisome subunits, which assemble into a special type of crystalloid P-protein found uniquely in Fabaceae (23–28). Forisomes differ from conventional P-proteins because they can undergo a reversible switch between condensed spindle-shaped and dispersed plug-forming states, triggered by a calcium influx

Author contributions: A.M.E., D.P., and G.A.N. designed research; A.M.E., S.B.J., S.Z., B.M., and U.N. performed research; A.M.E., S.B.J., S.Z., B.M., B.R., V.K., D.P., and G.A.N. analyzed data; and A.M.E., R.M.T., and D.P. wrote the paper.

The authors declare no conflict of interest.

*This Direct Submission article had a prearranged editor.

Data deposition: The sequences reported in this paper have been deposited in the GenBank database, www.ncbi.nlm.nih.gov/genbank/ [accession nos. JX119092 (PNtSEO1), JX119093 (NtSEO1), JX119094 (PNtSEO2), JX119095 (NtSEO2), JX119096 (PCmSEO1), and JX119097 (CmSEO1).

[1]To whom correspondence should be addressed: dpruefer@uni-muenster.de.

See Author Summary on page 11084 (volume 109, number 28).

This article contains supporting information online at www.pnas.org/lookup/suppl/doi:10.1073/pnas.1202999109/-/DCSupplemental.

(29, 30). Genes encoding forisomes are expressed in immature sieve elements (24, 28, 31, 32), and the corresponding protein assemblies share several structural and functional characteristics with conventional P-proteins (33, 34). SEO proteins contain three conserved domains: the SEO N-terminal domain (SEO-NTD), a potential thioredoxin fold, and the SEO C-terminal domain (SEO-CTD). The presence of all three domains is required for inclusion in the SEO family because the individual domains can be present in otherwise unrelated proteins. We recently identified members of the *SEO* gene family in several non-Fabaceae dicotyledonous angiosperms, indicating that the *SEO* family is widespread and additionally encodes conventional nonforisome P-proteins (28, 35).

Here, we report a comprehensive characterization of non-Fabaceae *SEO* genes. We analyzed the expression of two *SEO* genes from tobacco (*Nicotiana tabacum*), investigated the location and behavior of NtSEO-GFP fusion proteins, studied the ultrastructure of NtSEO-derived protein complexes by transmission electron microscopy (TEM), and produced NtSEO-depleted tobacco plants by RNAi to determine the function of structural P-proteins in wound sealing. Our data provide direct evidence that *SEO* genes encode P-proteins in tobacco and finally confirm their translocation-blocking activity following injury. The molecular analysis of a squash *SEO* gene led to the same conclusion. Therefore, our studies confirm the identity and uniformity of structural phloem proteins in dicotyledonous plants as well as the extensively discussed exceptional role of extrafascicular P-proteins in cucurbits.

Results

Identification of Tobacco *SEO* Genes. The *SEO* gene family originally was restricted to genes encoding forisomes but now also includes genes from non-Fabaceae plants, which do not possess forisomes. Because forisomes and conventional P-proteins have several characteristics in common, we previously speculated that the *SEO* gene family also encodes these widespread nonforisome P-proteins (28, 35). We therefore used previously published SEO sequences as BLAST queries to search for homologous sequences in tobacco, and this search revealed several matching ESTs. Genome walking and amplification using the RT-PCR led to the isolation of two genomic clones and corresponding cDNAs, representing the *Nicotiana tabacum SEO* genes *NtSEO1* and *NtSEO2*. The encoded proteins, NtSEO1 and NtSEO2, contain the three conserved SEO domains (Fig. S1) (28) and therefore belong to the SEO family.

Expression of *NtSEO* Genes Is Restricted to Immature Sieve Elements. The expression profiles of the two *NtSEO* genes were determined by RT-PCR using total RNA from young leaves, stems, roots, and flowers. The *SEO* mRNA levels were normalized against *GAPDH* mRNA as an internal control. The expression profiles were very similar, with strong expression in all analyzed tissues (Fig. 1*A*). Several *SEO* genes are known to be expressed in immature sieve elements (28). Accordingly, we observed age-dependent regulation of both *NtSEO* genes, each showing a strong decline in mRNA levels in maturing leaves undergoing source-sink transition (Fig. S2) (36). More precise spatiotemporal profiles were obtained for *NtSEO1* and *NtSEO2* by promoter analysis using reporter constructs. Initially, we amplified a 1,450-bp genomic sequence upstream of *NtSEO1* (P_{NtSEO1}) and fused this fragment to the *Escherichia coli uidA* gene encoding β-glucuronidase (GUS). In $P_{NtSEO1}GUS$ transgenic plants, GUS activity appeared to be restricted to the vascular bundle (Fig. 1*B*), confirming the anticipated spatiotemporal expression pattern already observed for other *SEO* genes in sieve elements (24, 28, 31, 32).

We also expressed an endoplasmic reticulum (ER)-targeted, KDEL-tagged version of GFP (GFP_{ER}) using the promoter elements of both genes to refine the localization data further. Transgenic plants expressing constructs $P_{NtSEO1}GFP_{ER}$ and $P_{NtSEO2}GFP_{ER}$ were analyzed by confocal laser scanning microscopy (CLSM). Cross-sections of tobacco petioles from immature leaves (Fig. 1*C* shows $P_{NtSEO1}GFP_{ER}$ as an example) clearly indicated that GFP fluorescence was restricted to phloem tissue within the vascular bundle. Longitudinal sections of the same tissues revealed nearly identical patterns of GFP activity in cellular networks representing consecutively connected sieve elements (Fig. 1*D* shows $P_{NtSEO2}GFP_{ER}$ as an example). Under higher magnification, single cells showed the typical morphology of sieve elements. This fact was confirmed by aniline blue

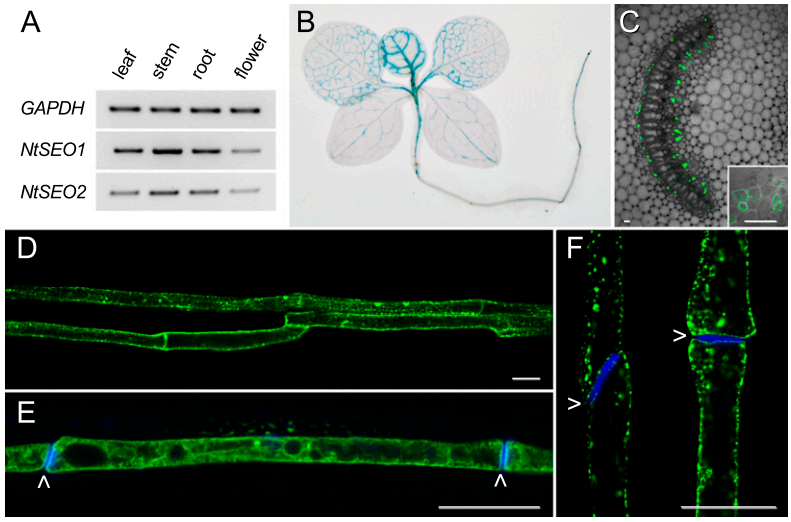

Fig. 1. Analysis of *NtSEO* expression in tobacco. (*A*) *NtSEO*-specific fragments were amplified from cDNA generated from the total RNA of leaves, stems, roots, and flowers. The tobacco *GAPDH* gene was used as a control. (*B*) Histochemical localization of GUS activity in a $P_{NtSEO1}GUS$ transgenic tobacco seedling. (*C*) Cross-section of a $P_{NtSEO1}GFP_{ER}$ transgenic tobacco petiole shown as an overlay of GFP_{ER} fluorescence and the corresponding transmitted light picture. (*Inset*) A single phloem bundle is shown in higher magnification. (*D* and *E*) Longitudinal sections of $P_{NtSEO2}GFP_{ER}$ transgenic tobacco petioles. (*F*) Longitudinal section of a $P_{NtSEO1}GFP_{ER}$ transgenic tobacco petiole. Sieve plates are stained with aniline blue in *E* and *F* (indicated by arrowheads). (Scale bars: 30 μm.)

staining, which labels sieve plates by their accumulation of callose (37). In both $P_{NtSEO1}GFP_{ER}$ and $P_{NtSEO2}GFP_{ER}$ transgenic plants, fluorescent cells were clearly identified as sieve elements connected to each other through sieve plates (Fig. 1 *E* and *F*). GFP fluorescence was detected in nucleated immature sieve elements containing vacuoles (Fig. 1*E*) but also in functional mature sieve elements (Fig. 1 *D* and *F*) because of GFP retention in the ER. However, no fluorescence was observed in functional mature sieve elements from transgenic tobacco plants expressing humanized *Renilla* GFP (hrGFP) (i.e., lacking an ER retention signal) under the control of the same promoter elements (Fig. S2). Therefore the promoter activities are consistent with the spatiotemporal formation of structural P-proteins.

NtSEO Proteins Tagged with a Fluorescent Reporter Assemble in Native P-Proteins in a Homologous Background. We next set out to characterize the assembly of NtSEO1 and NtSEO2 by expressing them with fluorescent tags, allowing the assembled complexes to be detected by CLSM. Each of the *NtSEO* genes therefore was expressed as a fusion with *hrGFP* under the control of the corresponding promoter. The resulting plant lines were designated "P_{NtSEO1}*NtSEO1:hrGFP*," "P_{NtSEO2}*NtSEO2:hrGFP*," and "P_{NtSEO2}*hrGFP:NtSEO2*" (Fig. S3).

In the first set of experiments, 10 independent P_{NtSEO1}*NtSEO1:hrGFP* and P_{NtSEO2}*NtSEO2:hrGFP* transgenic tobacco lines were regenerated and analyzed by CLSM. Although NtSEO1:hrGFP fluorescence was strong, NtSEO2:hrGFP produced only weak fluorescence, suggesting impaired retention within sieve elements when the reporter was placed as a C-terminal fusion. Therefore, transgenic plants expressing an analogous N-terminal hrGFP fusion were prepared, resulting in the construct P_{NtSEO2}*hrGFP:NtSEO2*. In the sieve elements of transgenic lines, the constructs P_{NtSEO1}*NtSEO1:hrGFP* (Fig. 2 *A*, *C–H*, and *L*) and P_{NtSEO2}*hrGFP:NtSEO2* (Fig. 2 *J* and *K*) induced the formation of similar fluorescent protein assemblies. Large protein bodies (always one per cell) resembling the typical P-protein bodies found in differentiating sieve elements were identified in several immature sieve elements (Fig. 2*A*) comparable to those structures observed in wild-type tobacco explants stained with amido black (Fig. 2*B*). Smaller, plasma membrane-associated fluorescent agglomerates also were detected in some mature sieve elements (Fig. 2 *C* and *J*), but most of the fluorescence was localized to sieve plates (Fig. 2 *D–H*, *K*, and *L*). The accumulations clearly were composed of diffusely arranged fibrils (Fig. 2 *F* and *G*) and appeared to form slime strands (Fig. 2*H*) predominantly associated with prominent plugs (Fig. 2 *K* and *L*). The same proteinaceous assemblies representing P-protein structures typically found in wounded tissue

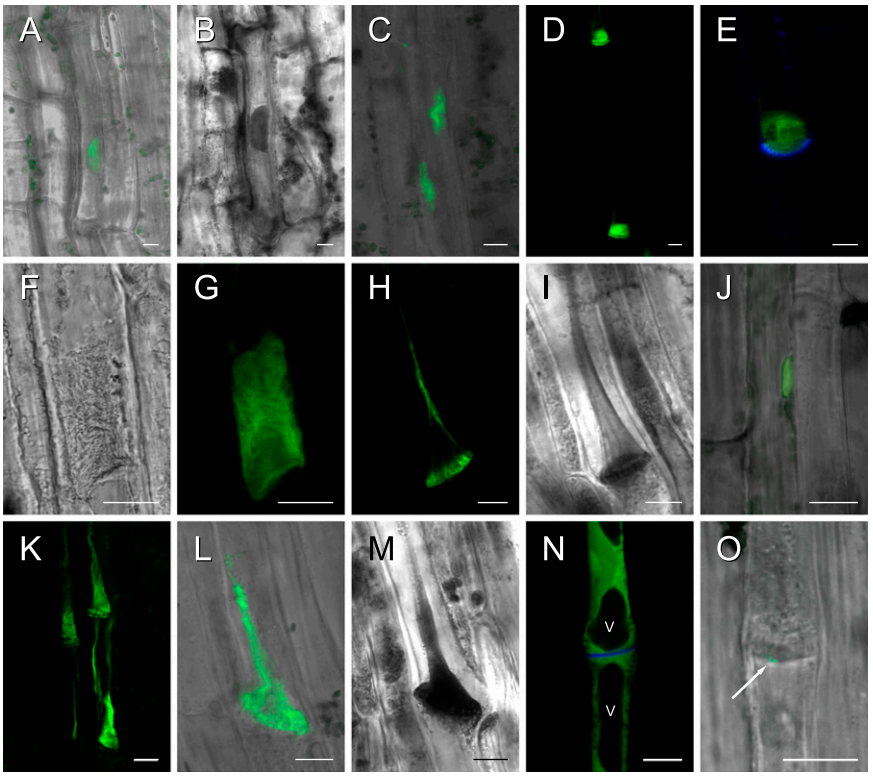

Fig. 2. Confocal images of NtSEO:hrGFP fluorescence and controls in transgenic tobacco plants. (*A, C–E, G,* and *H*) hrGFP fluorescence in P_{NtSEO1}*NtSEO1:hrGFP* transgenic tobacco plants. (*A* and *B*) P-protein bodies in immature sieve elements of transgenic (*A*) and wild-type tobacco (*B*) after amido black staining. (*C–H*) In mature sieve elements, fluorescent agglomerates were associated occasionally with the plasma membrane (*C*) but were observed more often on sieve plates (*D–H*). Under transmitted (*F*) and fluorescent (*G*) light, NtSEO1:hrGFP plugs appeared to be composed of fibrillar material. Formation of fluorescent transcellular slime strands was observed also (*H*), corresponding to P-protein structures in wild-type explants stained with amido black (*I*). (*J* and *K*) hrGFP fluorescence in P_{NtSEO2}*hrGFP:NtSEO2* transgenic tobacco. (*J*) Parietal agglomerates observed in various sieve elements clearly exhibited hrGFP fluorescence. (*K*) Plugs and associated slime strands were observed also. (*L* and *M*) An NtSEO1:hrGFP fluorescent plug (*L*) compared with native P-proteins in wild-type tobacco plants (*M*) stained with amido black. (*N*) hrGFP expression driven by P_{NtSEO1} exclusively resulted in a cytoplasmic fluorescence of immature sieve elements (immature state indicated by vacuoles, identified by the arrowhead), whereas no fluorescence was detected in mature sieve elements. (*O*) In $P_{MtSEO1\text{-}F1}$*MtSEO1-F1:hrGFP* transgenic tobacco, hrGFP fluorescence was observed occasionally as small accumulations in the boundary area of sieve plates (indicated by arrow) but was totally absent in most explants. In *A, C, J, L,* and *O*, overlays of hrGFP fluorescence and transmitted light images show the location of the hrGFP-tagged NtSEOs or the MtSEO-F1:hrGFP control in the cell. In *E* and *N* sieve plates were stained with aniline blue and are shown as overlays with hrGFP images. (Scale bars: 10 μm.)

were observed in wild-type tobacco sieve elements stained with amido black (Fig. 2 *I* and *M*).

To exclude the possibility that the observed structures were experimental artifacts caused by the incorporation of hrGFP into native P-protein structures, we expressed the fluorescent protein on its own using the *NtSEO1* promoter in transgenic tobacco (P_{NtSEO1}*hrGFP*) (Fig. S3). Cytoplasmic fluorescence was observed in young, nontransporting sieve elements with several large vacuoles (Fig. 2*N*) but no longer was evident in mature sieve elements, indicating that the hrGFP was translocated along with other soluble molecules (38). To exclude the possibility that NtSEO fusions were retained in sieve elements simply because of their size, we expressed hrGFP fusions of a related structural protein in tobacco as a control. The *MtSEO-F1* sequence in $P_{MtSEO\text{-}F1}$*MtSEO-F1:hrGFP* (Fig. S3) encodes a forisome subunit similar in size and composition to the NtSEO proteins (Fig. S1). CLSM analysis of transgenic plants revealed fluorescence patterns distinct from those obtained with the NtSEO fusions. In most cases, no hrGFP fluorescence could be detected in sieve elements, but small fluorescent deposits were observed occasionally in slow-flow areas at the periphery of sieve plates (Fig. 2*O*). These results show that most MtSEO-F1 fusion proteins were expressed but were translocated and never assembled into P-protein–like structures, clearly demonstrating that the retention of NtSEO:hrGFP fusion proteins did not reflect nonspecific, size-dependent effects.

Transient Coexpression in a Heterologous Background Provides Insight into P-Protein Assembly. To study the process of NtSEO assembly in the absence of native phloem components, we expressed *NtSEO1* and *NtSEO2*, with and without fluorescent tags, by agroinfiltration in *Nicotiana benthamiana* leaves, resulting in transient expression in epidermal cells (39). Fig. S4 shows a schematic representation of the constructs used in these experiments. All coding sequences were placed under the control of the double-enhanced *Cauliflower mosaic virus* 35S (CaMV 35S) promoter to allow expression in epidermal cells, and for visualization the NtSEO proteins were expressed as either N- or C-terminal fusions to YFP Venus. We recently reported that two *M. truncatula* SEO proteins (MtSEO-F1 and MtSEO-F4) assemble into spindle-like structures similar to native forisomes (Fig. 3*A*) when coexpressed as tagged and untagged versions in *N. benthamiana* (25, 27), demonstrating the validity of this approach for the analysis of NtSEO assembly.

In the first set of experiments, *NtSEO1* and *NtSEO2* were expressed in different combinations along with a *Venus* control, and the resulting fluorescence was analyzed 3 d postinfiltration (dpi). Although the expression of Venus resulted in exclusively cytoplasmic fluorescence (Fig. 3*B*), and the expression of single-tagged NtSEO proteins led to either cytoplasmic fluorescence (Fig. S4*B*) or smaller heteromorphic agglomerates (Fig. S4*C*), probably because of the fused reporter (25), both NtSEO1 and NtSEO2 formed P-protein–like complexes in *N. benthamiana* epidermal cells when coexpressed as tagged and untagged versions, respectively. These complexes often appeared to be located close to the plasma membrane but were freely present in the cytoplasm, as shown by combinatorial expression with a monomeric RFP (mRFP) cytoplasmic marker (Fig. 3*C*). Chimeric assemblies of NtSEO1 + NtSEO1:Venus (Fig. 3 *D–F*) and NtSEO2 + Venus:NtSEO2 (Fig. 3 *G–I*) appeared to comprise fibrillar subunits predominantly oriented along an imaginary longitudinal axis (Fig. 3 *D*, *E*, *G*, and *H*). This orderly arrangement also was observed in the perpendicular (cross-sectional) view (Fig. 3 *F* and *I*) showing the parallel fibrillar subunits. Fluorescent agglomerates were observed first at 2 dpi and increased in size until 3–4 dpi. These complexes were observed only when Venus was fused to the C terminus of NtSEO1 or the N terminus of NtSEO2, mirroring the results in the transgenic plant experiments described above.

Analysis of NtSEOs by Electron Microscopy Shows Ultrastructural Conformance with Structural P-Proteins. We next used TEM to determine the ultrastructure of putative P-proteins derived from the *NtSEO* genes expressed in *N. benthamiana* epidermal cells. Nontagged NtSEO2 (Fig. S4) was expressed in *N. benthamiana* epidermal cells as described above, and infiltrated leaf discs were harvested 3 dpi. TEM images revealed an abundance of fibrillar components normally absent from epidermal cells. The subunits frequently were assembled into orderly complexes apparent in both transverse (Fig. 3*J*) and longitudinal (Fig. 3*K*) sections, similar to the fluorescent infiltration complexes described above. Most importantly, the ultrastructural characteristics (filament assembly and size of single fibrils) revealed by TEM perfectly matched those observed for native tobacco P-protein bodies in previous studies (5), strongly suggesting that NtSEOs are structural P-proteins.

NtSEO-Knockdown Plants Contain only Residual Levels of P-Protein. To demonstrate conclusively that structural P-proteins in tobacco are indeed NtSEO proteins and to evaluate their extensively discussed functions, we generated *NtSEO*-RNAi lines lacking the ability to produce normal amounts of the corresponding proteins. We amplified 500-bp target sequences for both *NtSEO1* and *NtSEO2* and used them to generate constructs allowing the production of *NtSEO*-specific hairpin RNAs under the control of the corresponding sieve element-specific promoters. Transgenic tobacco plants carrying T-DNA insertions for both RNAi constructs were generated and analyzed for *NtSEO1* and *NtSEO2* expression by real-time quantitative RT-PCR. Among 25 regenerated plant lines, two lines were selected based on their efficient knockdown of both *NtSEO* genes (Fig. 4*A*). Line N produced *NtSEO1* and *NtSEO2* mRNAs at 0.14% and 1.27% of wild-type levels, respectively. Similarly, line T produced *NtSEO1* and *NtSEO2* mRNAs at 0.20% and 0.14% of wild-type levels, respectively. Despite the depletion of both mRNAs, neither of the transgenic lines presented an obvious phenotype during cultivation.

Transgenic tissue was harvested for microscopic analysis toward the end of the vegetative phase. To visualize the amount of P-protein in sieve elements, explants were prepared and stained with amido black. Dicot phloem explants normally are characterized by the abundance of dispersed P-protein material within and emerging from severely damaged sieve elements at the surface of explants (22), as was evident in wild-type tobacco samples (Fig. 4*B*, see also Fig. 2 *B*, *I*, and *M*). In contrast, no accumulation of stained P-protein material was detected at the surface of explants from lines N and T, and the decrease of P-protein structures also was obvious at the cellular level. Neither the immature sieve elements (compare Figs. 4*C* and 2*B*) nor the mature sieve tubes (compare Figs. 4*D* and 2*M*) of lines N and T contained prominent P-protein structures.

Phloem explants from petioles of wild-type and transgenic plants then were analyzed by TEM to determine their ultrastructural properties (Fig. 4 *E–H*). In wild-type sieve elements, the P-protein filaments generally were concentrated on one side of a sieve plate (Fig. 4*E*), evidently occluding sieve pores (Fig. 4*F*). In contrast, the lumen of sieve tubes from RNAi plants was essentially devoid of P-proteins (Fig. 4*G*), with only residual filaments at sieve plates (Fig. 4*H*). This observation confirmed that RNAi achieved significant NtSEO knockdown at the protein level and confirmed the identity of NtSEO proteins as tobacco P-proteins.

NtSEO-Knockdown Plants Show Enhanced Bleeding After Wounding. If the role of P-proteins is, as suggested, to seal the sieve pores of damaged sieve tubes and prevent the loss of photoassimilate,

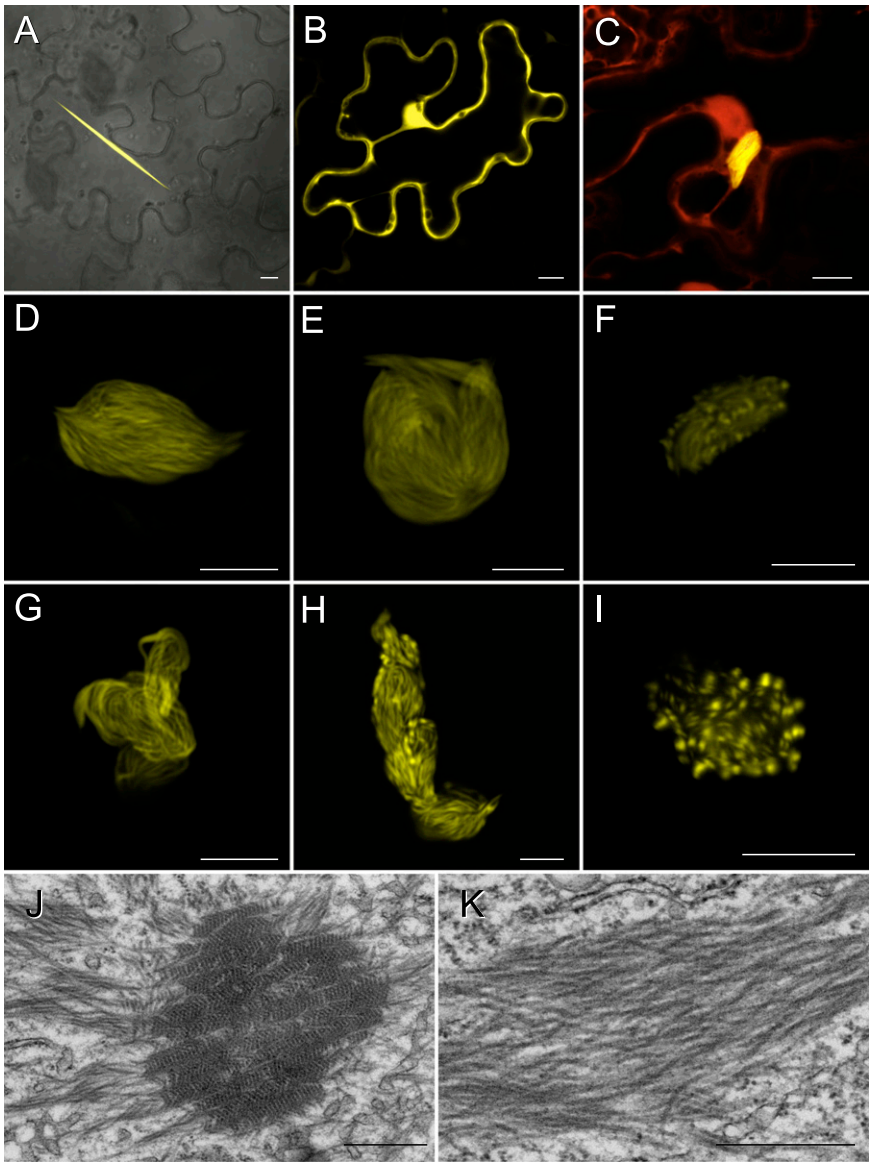

Fig. 3. SEO protein bodies in epidermal cells of agroinfiltrated *N. benthamiana* leaves. (*A*) The combined expression of MtSEO-F1 + MtSEO-F1:Venus leads to the assembly of forisome-like structures. (*B*) The expression of reporter Venus results in cytoplasmic fluorescence. (*C*) Localization of a protein body composed of NtSEO1 + NtSEO1:Venus within an epidermal cell when coexpressed with cytoplasmic mRFP. (*D–F*) Fluorescent protein bodies observed for the combination NtSEO1 + NtSEO1:Venus. The arrangement of fluorescent fibrils is visible in both the longitudinal (*D* and *E*) and transverse views (*F*). (*G–I*) Protein bodies composed of NtSEO2 + Venus:NtSEO2. Fluorescent agglomerates are shown in the longitudinal (*G* and *H*) and transverse (*I*) views. (*J* and *K*) NtSEO2-derived complexes in *N. benthamiana* epidermal cells exhibit the typical ultrastructural characteristics of tobacco P-proteins in both the transverse (*J*) and longitudinal (*K*) views. (Scale bars: 10 μm for *A–I*; 0.5 μm for *J* and *K*.)

then lines N and T (which do not produce normal levels of P-proteins) should lack this form of protection and should lose more assimilate than wild-type plants after wounding. When the leaves from RNAi plants were cut at the petioles, we did not observe a visible increase in the amount of phloem sap accumulating at the cut surfaces in comparison with corresponding wild-type plants. We therefore compared exudation rates from the cut leaves of wild-type tobacco and the *NtSEO*-RNAi lines. Efficient and long-term exudation usually is achieved by adding EDTA to the medium; EDTA is thought to inhibit or at least reduce the formation of wound callose in sieve pores by chelating Ca^{2+} (40, 41). However, callose depositions in sieve pores are known to promote the long-term sealing of sieve plates (42, 43), and at least several minutes pass before the pores are fully sealed (44). In contrast, P-proteins are thought to represent a rapid wound-sealing mechanism, so we measured the exuded sugars from wild-type tobacco plants and the *NtSEO*-RNAi lines over a short time frame (10 min directly after cutting). The impact of callose deposition over such a short period would be negligible, allowing us to avoid the use of EDTA or comparable reagents, which are thought to generate experimental artifacts (45).

Exudation experiments were carried out as shown in Fig. S5 using 7-wk-old plants from *NtSEO*-RNAi lines N ($n = 48$) and T ($n = 57$), compared with wild-type control plants ($n = 57$). Three leaves from each plant were exuded into the same vial, and all samples subsequently were lyophilized and dissolved in water. In tobacco, assimilate is allocated predominantly in the form of sucrose (46). We therefore used the Sucrose/D-Glucose/D-Fructose Kit (Roche) to determine the D-glucose concentration of all samples before and after the enzymatic hydrolysis of sucrose. The

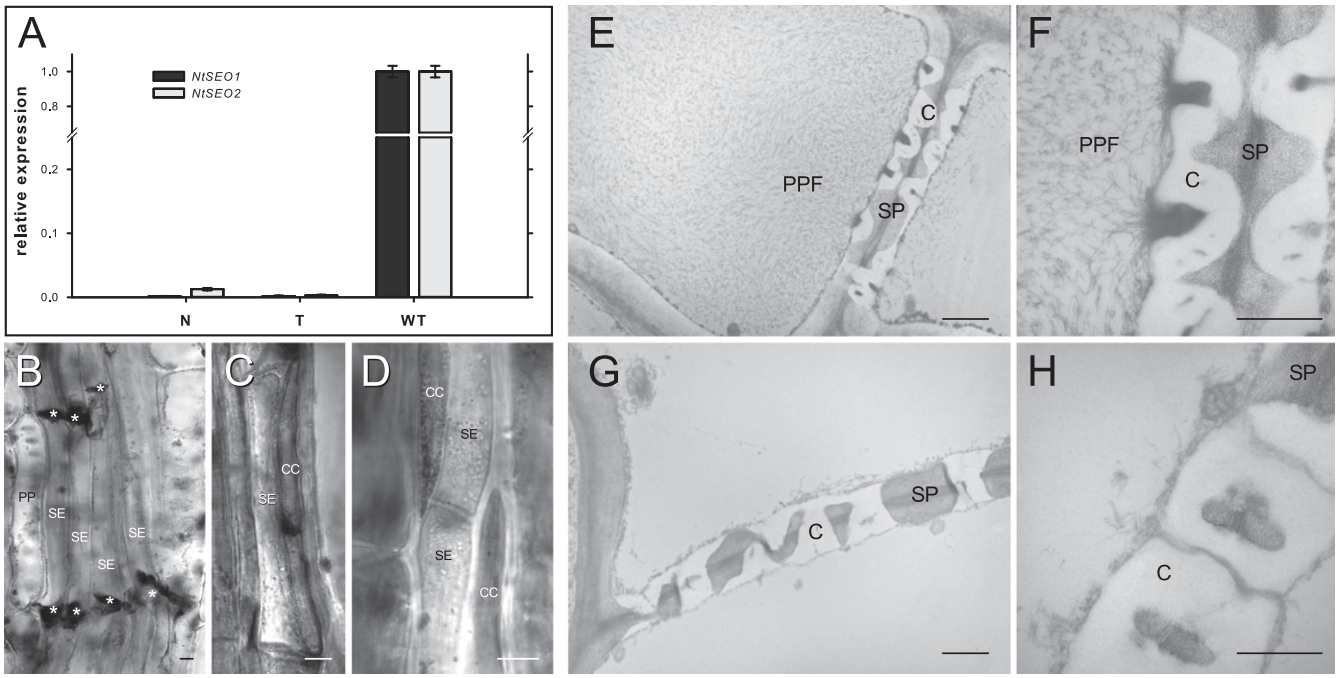

Fig. 4. Analysis of *NtSEO*-RNAi lines. (*A*) Expression of *NtSEO1* and *NtSEO2* in young leaves of T0 plants representing two independent *NtSEO*-RNAi lines (N and T) and corresponding wild-type (WT) plants. The expression levels of *NtSEO1* and *NtSEO2* in wild-type leaves were set at 1 for relative measurements. (*B–D*) CLSM images of tobacco petiole explants stained with amido black. Wild-type explants generally were characterized by darkly stained P-protein material emerging from severely damaged sieve elements (*B*; sieve plates are indicated by asterisks), which was never observed in *NtSEO*-RNAi lines (*C* and *D*). The RNAi lines lacked the typical P-protein bodies of immature sieve elements (*C*), and no plugs were observed at sieve plates of mature sieve tubes (*D*, showing RNAi line N as an example). (*E–H*) TEM analysis of sieve elements from wild-type tobacco and *NtSEO*-RNAi line N, revealing abundant P-protein filaments in wild-type sieve elements (*E*) clearly occluding sieve pores (*F*). In contrast, sieve elements in RNAi plants were essentially devoid of P-proteins (*G*), with only residual amounts detected close to sieve plates (*H*); C, callose; CC, companion cell; PP, phloem parenchyma; PPF, P-protein filaments; SE, sieve element; SP, sieve plate. (Scale bars: 10 μm in *B–D*, 1 μm in *E* and *G*, and 0.5 μm in *F* and *H*.)

difference between the values allowed us to distinguish glucose originating from damaged cells at the cut surface from glucose derived from sucrose, the latter most probably representing assimilates exuding from damaged sieve tubes (Fig. 5; details are provided in Table S1 and Fig. S6).

In the wild-type tobacco samples, most of the detected glucose was derived from the surrounding damaged tissue rather than from assimilated sucrose, demonstrating the efficiency of phloem sealing in these plants (Fig. 5 and Fig. S6). In contrast, the average sucrose content was up to nine times higher in the exudates from RNAi-lines N and T, despite the reduced and variable potency of the knockdown effects in T1 progeny compared with the parental plants (Fig. 5). To exclude the possibility that the increased sucrose concentrations in exudates from *NtSEO*-RNAi plants reflected abnormal sucrose allocation in the transgenic lines, we also harvested and shredded petiole sections from wild-type and RNAi plants and determined the total sucrose content, which was consistent across all analyzed samples (Table S2). Therefore, the differences we observed were not caused by the deregulated accumulation of transport sugars in *NtSEO*-RNAi lines. Indeed, the uniform total sucrose concentrations in petiole tissues provided further evidence that the higher sucrose levels in the exudates from transgenic plants could be explained only by the loss of sucrose from damaged translocating sieve tubes. As stated above, the *NtSEO*-RNAi lines lacked overt macroscopic or microscopic phenotypes (growth and development, phloem structure, and callose accumulation were normal; see Fig. 4) and differed only in lacking P-proteins in the sieve elements. Therefore, the enhanced bleeding of *NtSEO*-RNAi lines appears to be a direct consequence of the reduced P-protein content. Our exudation analysis finally confirms the extensively discussed role of P-proteins and offers functional proof that these structural proteins indeed contribute to the efficient and rapid sealing of the phloem system after injury, preventing the loss of photosynthate.

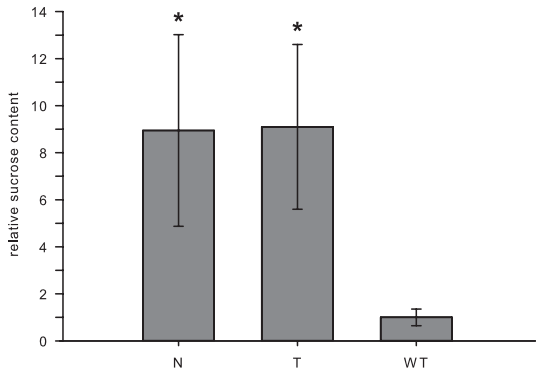

Fig. 5. Analysis of exudation rates in *NtSEO*-RNAi lines and wild-type tobacco plants. The average exudation rate of two independent *NtSEO*-RNAi lines (N and T) and corresponding wild-type plants (WT) was determined by the amount of sucrose exuded from leaves in the first 10 min after cutting. The mean value of sucrose exuded from wild-type plants was set at 1 for relative measurements. Results shown represent mean ± SD; $n_N = 48$, $n_T = 57$, $n_{WT} = 57$; $^*P \leq 0.001$, Mann–Whitney *u* test. Details are provided in Table S1 and Fig. S6.

Identification and Characterization of a *SEO* Gene from Squash. As discussed above, the classification of SEO proteins as structural P-proteins appears to contradict the P-protein model based on PP1 from *C. maxima*, which was the first P-protein to be characterized. However, Zhang et al. (22) recently isolated P-protein

plugs from fascicular sieve elements of squash plants and generated peptides (Fig. 6*A*) leading to the identification of a phloem sap sequence (GenBank accession no. FG227702) matching an uncharacterized protein with a speculative role in wound sealing. Applying the assignment criteria proposed by Rüping et al. (28), we were able to identify this partial sequence as a *SEO* gene fragment. We used the sequence data to isolate a genomic clone and corresponding cDNA and found the typical characteristics of a *SEO* gene, including the conserved exon-intron structure and the presence of the three SEO-specific domains (Fig. 6*A*). Furthermore, GFP_{ER}-based promoter studies in transgenic *C. maxima* roots showed that expression was restricted to immature sieve elements (Fig. 6*B*). We therefore named the gene "*CmSEO1*."

Following the strategy we used for *NtSEO1* and *NtSEO2*, we next set out to determine whether Venus-tagged CmSEO1 assembled into typical conventional P-protein structures. Therefore CmSEO1 was expressed as a Venus fusion protein under the control of the corresponding promoter in the homologous background. CLSM analysis of longitudinal transgenic squash root sections confirmed incorporation of the Venus-tagged CmSEO1 fusion protein into proteinaceous plugs formed at the sieve plates (Fig. 6*C*), reflecting the typical characteristics of conventional P-proteins after wounding.

Discussion

***SEO* Genes Encode Structural P-Proteins That Influence Translocation.** P-proteins have been identified in many dicotyledonous plants, and their structure and function during maturation and sieve plate plugging after wounding appear highly conserved even in distantly related species (1, 7, 9, 12, 13). Despite the characterization of special types of P-proteins, namely the Fabaceae-specific forisomes and Cucurbitaceae-specific PP1, the molecular nature of structural P-proteins has remained poorly understood. Therefore we carried out a comprehensive characterization of *SEO* genes from the non-Fabaceae species *N. tabacum*. Our experiments provide conclusive evidence that indeed this widespread gene family does encode, in addition to forisomes, the structural P-proteins of dicotyledonous angiosperms, and we also provide conclusive data to confirm their long-debated function as key players in the rapid sealing of injured sieve tubes.

We cloned two *SEO* genes from tobacco (*NtSEO1* and *NtSEO2*) and showed that their expression profiles (Fig. 1 and Fig. S2) mirrored the rapid assembly of conventional P-protein bodies in immature phloem cells (5). Furthermore, the expression of *NtSEO* genes as hrGFP fusions in a homologous genetic background resulted in the assembly of fluorescent proteinaceous agglomerates that reflected the characteristic morphology of structural P-proteins (Fig. 2). In immature tobacco sieve elements, P-protein maturation is characterized by the formation of large protein bodies (5, 10), and similar fluorescent protein complexes were identified in the transgenic lines. The most striking demonstration of P-protein–like activity was the behavior of the NtSEO fusions after wounding: The fluorescent complexes in wounded transgenic plants formed distinctive plugs on most sieve plates, and these plugs sometimes even terminated with gel-like transcellular strands, as is consistent with the known characteristics of P-proteins (47, 48). The frequent observation of plugged sieve plates instead of parietal agglomerates in mature sieve tubes probably reflects the damage caused by explant preparation before CLSM and is not indicative of the status quo in uninjured transgenic plants. The immense plugs we observed in the transgenic plants should reduce or even prevent translocation, causing severe physiological stress. However, because there were no obvious differences in phenotype between transgenic plants and wild-type controls, we conclude that the fluorescent proteins interact with their native counterparts in uninjured tissues, maintaining mass flow.

The constitutive combinatorial expression of tagged and untagged *NtSEO* genes in *N. benthamiana* epidermal cells led to the formation of fluorescent P-protein–like agglomerates comprising aligned fibrillar subunits (Fig. 3). This parallel arrangement was observed in both longitudinal and transverse sections of fluorescent protein bodies and exactly matches the documented formation of P-proteins in immature tobacco sieve elements (5). TEM images provided additional convincing evidence that the NtSEO-derived protein bodies in *N. benthamiana* epidermal cells had the same fibrillar ultrastructure as conventional P-proteins, with characteristic aggregated fibrillar subunits similar in size to the fibrils observed in tobacco phloem (5).

Finally, we established beyond doubt that P-proteins in tobacco are NtSEO proteins by generating *NtSEO*-knockdown lines by RNAi and noting that the immature and mature sieve elements in these lines were essentially devoid of P-protein structures (Fig. 4). The availability of P-protein–depleted tobacco plants also provided an opportunity to confirm the functional role of the widely distributed structural phloem components, a fact that has been controversially discussed since their discovery in the 19th century (49). There is general agreement that sieve pores connecting individual sieve elements normally are free of proteinaceous deposits and that the occluded sieve pores and large P-protein plugs often observed by microscopy reflect injuries caused during explant preparation and therefore represent the typical state after wounding. The detachment of parietal P-proteins and their accumulation on downstream sieve plates also has been demonstrated in vivo (1, 16) but provides only indirect evidence for a role in sieve tube sealing.

Recent studies on an *Arabidopsis* SEO protein even failed to demonstrate any effect of P-proteins on translocation, although

Fig. 6. Analysis of CmSEO1 from squash. (*A*) Deduced amino acid sequence of CmSEO1. Peptide sequences reported by Zhang et al. (22) are indicated in bold, and SEO-specific domains are shaded in yellow (SEO-NTD), blue (potential thioredoxin fold), and gray (SEO-CTD). (*B*) Sieve element-specific reporter expression in longitudinal section from a $P_{CmSEO1}GFP_{ER}$ transgenic squash root. (*C*) Venus fluorescence in $P_{CmSEO1}CmSEO1{:}Venus$ transgenic squash roots typically was observed in protein plugs at sieve plates. CC, companion cell; SE, sieve element; SP, sieve plate. (Scale bars: 10 μm.)

the small size of *Arabidopsis* sieve tubes was a drawback in these experiments (50). The challenge of addressing the function of P-proteins is rooted in the system itself, because the phloem has a high internal pressure and is well shielded within the plant, making it difficult to examine. In addition, P-proteins are not the only phloem components that may play a role in sieve tube sealing; for example, callose is thought to accomplish the long-term sealing of sieve plates (42, 43). Therefore we developed an assay based on phloem exudation of tobacco leaves to measure the extent of photoassimilate loss after injury (Fig. 5). We collected exudates for the first 10 min after wounding to minimize any impact of callose deposition and found that the P-protein–depleted RNAi lines exuded nine times more sucrose, on average, than wild-type plants. We excluded other potential sources of sucrose, indicating that NtSEO proteins have a major impact on translocation after wounding. When dicotyledonous plants are wounded, P-proteins detach from their parietal position in sieve elements and accumulate as viscous plugs (probably incorporating additional components, such as sieve element plastids) on downstream sieve plates. P-proteins become active immediately after injury, therefore preventing critical loss of photoassimilates in the delay before the sieve pores are sealed effectively with callose. Plants may gain further advantages from P-protein material forming large plugs covering the whole sieve plate area, because such plugs could prevent pathogens from invading wound sites and spreading systemically via the phloem. We have demonstrated clearly that P-protein accumulations block translocation following injury and that this protective mechanism is lost in the P-protein–depleted plant lines.

Distribution of *SEO* Genes Reveals the Uniformity of P-Proteins Among Dicotyledonous Angiosperms. Previous microscopy-based studies have characterized P-proteins of various plants in diverse states of differentiation and degrees of wounding, resulting in equally diverse and heterogeneous structures. Although indeed there are special types of P-proteins (e.g., the spindle-shaped forisomes found in Fabaceae), P-protein structures are similar in all dicotyledonous and many monocotyledonous angiosperms, indicating a potential phylogenetic relationship. We have confirmed this hypothesis by showing that the widespread *SEO* gene family encodes conventional structural P-proteins in addition to forisomes, as clearly demonstrated in the cases of *NtSEO1* and *NtSEO2*. The first P-proteins to be analyzed in detail were PP1 and the 24-kDa phloem lectin PP2, which are the main components of *C. maxima* exudates and are thought to be covalently linked (15). Cucurbits have long served as model plants in phloem research because their large phloem cells are well suited for microscopy and because they bleed profusely after injury, allowing the direct harvest of phloem exudates (51). Electron microscopy revealed the presence of P-protein filaments in *C. maxima* exudates (52); these filaments were assumed to be composed of PP1, although the ability of the protein to form stable structural components in vivo was debated because of its high turnover rate (53). PP1 is expressed initially in companion cells and then is transported into sieve elements, presumably via pore-plasmodesma units (19). The protein also was shown to be translocated over long distances, in contrast to the traditional concept that structural P-proteins form immobilized polymeric structures (20). Recently, a phloem-specific PP2 homolog from *Arabidopsis* (PP2-A1) was shown to be anchored to P-proteins and other phloem organelles rather than being a structural component of P-proteins (45), causing additional inconsistency regarding P-protein identity in angiosperms.

The abundance of sequence data clearly suggests that PP1 is unique, confirming the intrageneric conservation proposed by Clark et al. (19) but contradicting the existence of similar P-protein structures in all dicotyledonous angiosperms. Moreover, there is no sequence similarity between PP1 and the SEOs described herein, but the filaments of developing squash and tobacco P-protein bodies in assimilate-transporting sieve tubes appear almost identical (7). A significant step toward resolving this discrepancy was provided by Zhang et al. (22), who revealed significant differences between the fascicular (assimilate-transporting) and extrafascicular phloem system of *C. maxima*, the latter being unusual among higher plants. Additionally, droplets of exudate forming at the surfaces of cut stems or petioles, with PP1 and PP2 as the main proteinaceous components, were shown to originate predominantly from extrafascicular sieve tubes. In contrast, peptides from P-protein plugs isolated from fascicular phloem tissue led to the identification of an uncharacterized fragment of a protein with a proposed role in wound sealing (22). These peptide sequences helped us identify the protein as CmSEO1, which we included in our analysis to confirm our hypothesis that the widespread *SEO* gene family encodes subunits of conventional P-proteins in most angiosperms, including cucurbits (28, 35). Given its scarcity in sugar-transporting fascicular phloem and its abundance in extrafascicular phloem, PP1 is unlikely to belong to this group of conventional P-proteins. However, *Cucurbita* exudates, predominantly comprising the contents of the extrafascicular phloem, have a strong tendency to gel (54, 55), and this property may be attributable to PP1 (18). Therefore PP1-based gelling could represent an alternative wound-sealing mechanism to sieve plate occlusion by SEO proteins deployed in fascicular sieve tubes. These issues surely will be addressed in future experiments focusing on the differences between cucurbit extrafascicular and fascicular phloem systems to advance our understanding of the evolution of sieve tube sealing mechanisms in angiosperms, including the apparently unique role of PP1 in *Cucurbita*. Furthermore, most studies focusing on phloem sap composition have used exudates from cucurbit extrafascicular sieve tubes, and it would be most interesting to verify or even extend our current knowledge by analyzing fascicular phloem contents of angiosperms (22, 45). The knowledge that SEO proteins inhibit phloem exudation and the ability to generate plants depleted in these proteins provide a useful basis for such future experiments.

SEO genes encoding conventional P-proteins were identified by homology to the *M. truncatula SEO-F* genes, which encode forisome proteins. The sequence similarity indicates that forisomes and conventional P-proteins have a common evolutionary origin (28, 35). This notion is supported by several shared structural characteristics, such as their fibrillar composition (9, 56), their ultrastructure in the condensed and dispersed states (5, 57), their spatiotemporal expression profiles (24, 58), and their cellular function, although forisomes are unique in that the sealing of sieve plates is reversible (29). In this context, the Ca^{2+}-mediated dispersion of forisomes has been investigated in detail (30, 56), and it remains to be seen whether conventional P-proteins display any sensitivity to calcium or have any further functional similarities to forisomes.

Materials and Methods

Identification of *NtSEO1*, *NtSEO2*, and *CmSEO1*. The *SEO* genes described by Rüping et al. (28) were used as queries in a BLAST search (59) against GenBank to identify potential tobacco *SEO* sequences; the search yielded one EST fragment. The corresponding genomic gene sequence (*NtSEO1*) was obtained by genome walking using the BD Genome Walker Universal Kit (Clontech). The *NtSEO1* sequence was used in a subsequent BLAST search, revealing a second tobacco EST, which was used to isolate the *NtSEO2* gene by genome walking as described above. The full sequence of *CmSEO1* was obtained by genome walking using specific primers deduced from squash sap GenBank accession no. FG227702 (21). The corresponding coding sequence then was amplified by RT-PCR.

RT-PCR. For expression analysis, total RNA was isolated from young and old leaves, stems, roots, and flowers of tobacco (*N. tabacum* cv. SR-1), using the NucleoSpin RNA Plant Kit (Macherey-Nagel). Reverse transcription was per-

formed with SuperScript II (Invitrogen) according to the manufacturer's instructions followed by RNA digestion (RNaseH; New England Biolabs). Intron-spanning gene fragments were amplified by 30 PCR cycles. The tobacco *GAPDH* gene (*NtGAPDH*, accession no. AJ133422) was amplified as an internal control.

For real-time quantitative RT-PCR experiments, RNA extraction from young leaves, followed by DNaseI (New England Biolabs) treatment, and reverse transcription were performed as described above. Real-time quantitative RT-PCR was carried out using a CFX96 Real-Time System Cycler (Bio-Rad) and iQ SYBR Green Supermix (Bio-Rad). Reference genes *L25* (encoding L25 ribosomal protein) and *EF-1α* (encoding elongation factor 1α) were used as internal controls to normalize expression (60). Expression was determined in triplicate, and relative expression levels of target genes were analyzed using Bio-Rad CFX Manager 2.1. The integrity of all constructs was verified by sequencing. All primers used are given in *SI Materials and Methods*.

Stable Transformation of Tobacco Plants. All binary vectors used for stable plant transformation were introduced into *Agrobacterium tumefaciens* strain LBA4404 (61) by electroporation. Tobacco plants were transformed according to established protocols (62). For the RNAi experiments, *A. tumefaciens* cultures carrying pBP_{NtSEO1}hp*NtSEO1* or pBP_{NtSEO2}hp*NtSEO2* were cultivated separately and mixed immediately before the inoculation of tobacco leaves.

***NtSEO* Promoter Analysis.** All cloning steps performed to obtain promoter-reporter constructs are described in *SI Materials and Methods*. Sterilized seeds from P_{NtSEO1}*GUS* transgenic tobacco plants were germinated on Murashige and Skoog medium (63) supplemented with 50 μg/mL kanamycin for selection. GUS activity in 2- to 3-wk-old seedlings was detected using 5-bromo-4-chloro-3-indolyl-β-D-glucuronide without an oxidative catalyst according to established protocols (64). Promoter-specific GFP_{ER} expression was analyzed by CLSM.

***SEO:hrGFP* Fusion Constructs for P-Protein Visualization in Transgenic Plants.** All fusion constructs were assembled in the pBS*hrGFP* vector series containing the hrGFP (65) coding sequence fused to the CaMV 35S terminator. Fusions were obtained for *NtSEO1*, *NtSEO2*, and, as a control, forisome subunit-encoding *MtSEO-F1* (24, 27). The detailed cloning procedure is given in *SI Materials and Methods*. Transgenic plants were analyzed by CLSM.

Agroinfiltration of *N. benthamiana* plants. For transient expression in *N. benthamiana* epidermal cells, all tagged and untagged pBatTL-*SEO* constructs and controls (all cloning steps are described in *SI Materials and Methods*) were introduced into *A. tumefaciens* strain GV3101 pMP90 by electroporation. Young leaves from 4-wk-old plants were infiltrated simultaneously with *A. tumefaciens* strains GV3101 pMP90 (containing the pBatTL vectors) and C58C1 [carrying the pCH32 helper plasmid encoding the *Tomato bushy stunt virus* RNA-silencing suppressor p19 (39)]. After 3 d, infiltrated leaf discs were analyzed by CLSM.

Generation of Transgenic Squash Roots. To visualize GFP_{ER} expression under the control of P_{CmSEO1} and the CmSEO1:Venus fusion protein *in planta*, constructs $pBP_{CmSEO1}GFP_{ER}$ and $pB_{PCmSEO1}$*CmSEO1:Venus* (cloning steps are described *SI Materials and Methods*) were introduced into *Agrobacterium rhizogenes* strain NCPPB2659. Transgenic squash roots generated as previously described (66) were analyzed by CLSM.

CLSM and Imaging. Thin explants from stems or petioles (tobacco), leaf discs (*N. benthamiana*), or roots (squash) were analyzed by CLSM using a Leica TCS SP5× microscope with excitation/emission wavelengths of 488/500–580 nm for the visualization of all GFP derivatives, 514/540–580 nm for the detection of Venus, and 549/570–630 nm for the detection of mRFP. Sieve plates were stained with 0.01% aniline blue according to established protocols (67) and visualized at excitation/emission wavelengths of 364/470–530 nm. Native P-proteins in thin tobacco stem sections were stained with 1% (wt/vol) amido black (Roth) in 7% (vol/vol) acetic acid for 2 min and viewed under transmitted light.

TEM. For the ultrastructural analysis of infiltration complexes, small discs were punched from infiltrated *N. benthamiana* leaves 3 dpi using a 4-mm disposable biopsy punch. Leaf discs were fixed in 2% (vol/vol) paraformaldehyde, 2% (vol/vol) glutaraldehyde for 2 h and then were incubated in 1% (vol/vol) osmium tetroxide for 1 h (68). After dehydration in ethanol, the samples were equilibrated gradually in acetone, embedded in Agar Low Viscosity Resin (Plano GmbH) for 6 d, and polymerized in flat embedding molds at 60 °C for 20 h. Ultrathin sections were collected on copper slot grids as described by Moran and Rowley (69) and stained with lead citrate for up to 15 min (70). Sections were examined with an Hitachi H-7650 TEM operating at 100 kV, fitted with an AMT XR41-M digital camera (Advanced Microscopy Techniques).

Vascular tissue was isolated from the petioles of *NtSEO*-RNAi lines, fixed in 2% (vol/vol) glutaraldehyde and 3.5% (wt/vol) sucrose for 3 h, and then incubated in 1% (vol/vol) osmium tetroxide for 3 h. The samples were dehydrated in ethanol and embedded in LR White (Sigma). Sections were stained for 20 min by 2% (wt/vol) uranyl acetate in 50% (vol/vol) ethanol, followed by lead citrate for 3 min (70). The micrographs were recorded with a Philips CM10 transmission electron microscope operating at 80 kV.

Exudation Experiments. Tobacco plants (wild type and T1 progeny from NtSEO-RNAi lines N and T) were grown in a greenhouse with a 16-h photoperiod at 25 °C for 7 wk. Three leaves were removed from each plant (starting with the second or third true leaf; see Fig. S5 and Table S1) by cutting the petioles with a razor blade and were exuded successively into the same vial (containing 3 mL 1 mM MES, pH 7) for 10 min. Exudation experiments were carried out between zeitgeber times 5 and 9 for 3 d consecutively, with wild-type plants and RNAi lines exuded alternatively. After exudation, samples were frozen in liquid nitrogen and lyophilized. Freeze-dried samples were dissolved in 200 μL distilled water, and 25 μL of the solution was used to determine the quantity of D-glucose and sucrose, respectively, using the Sucrose/D-Glucose/D-Fructose Kit (Roche) according to the manufacturer's instructions.

To determine the total sucrose content of petioles, 1 g of petiole tissue was ground under liquid nitrogen, and the extraction and quantitation of sugars was carried out using the Sucrose/D-Glucose/D-Fructose kit (Roche) according to the manufacturer's instructions.

ACKNOWLEDGMENTS. We thank Dr. Guido Jach (Phytowelt GreenTechnologies GmbH) and Dr. H. Uhrig (University of Cologne) for kindly providing the pBatTL vector system; and Ann-Christin Müller, Raphael Soeur, and Claudia Hansen (Fraunhofer Institute for Molecular Biology and Applied Ecology), Ila Rouhara and Rainer Franzen (Max Planck Institute for Plant Breeding Research), and Ursula Malkus (Institute of Medical Physics and Biophysics, University of Muenster) for technical assistance. This work was supported in part by German Federal Ministry of Education and Research Grant 0312014, the Fraunhofer MAVO program, and Volkswagen Foundation Contract I/82 075.

1. Knoblauch M, van Bel AJE (1998) Sieve tubes in action. *Plant Cell* 10:35–50.
2. Will T, van Bel AJE (2006) Physical and chemical interactions between aphids and plants. *J Exp Bot* 57:729–737.
3. Cronshaw J (1981) Phloem structure and function. *Annu Rev Plant Physiol* 32:465–484.
4. Sjölund RD (1997) The phloem sieve element: A river runs through it. *Plant Cell* 9: 1137–1146.
5. Cronshaw J, Esau K (1967) Tubular and fibrillar components of mature and differentiating sieve elements. *J Cell Biol* 34:801–815.
6. Esau K, Cronshaw J (1967) Tubular components in cells of healthy and tobacco mosaic virus-infected *Nicotiana*. *Virology* 33:26–35.
7. Cronshaw J, Esau K (1968) P protein in the phloem of Cucurbita. I. The development of P-protein bodies. *J Cell Biol* 38:25–39.
8. Cronshaw J, Esau K (1968) P protein in the phloem of Cucurbita. II. The P protein of mature sieve elements. *J Cell Biol* 38:292–303.
9. Steer MW, Newcomb EH (1969) Development and dispersal of P-protein in the phloem of *Coleus blumei* Benth. *J Cell Sci* 4:155–169.
10. Wooding FBP (1969) P Protein and microtubular systems in *Nicotiana* callus phloem. *Planta* 85:284–298.
11. Evert RF, Eschrich W, Eichhorn SE (1973) P-protein distribution in mature sieve elements of *Cucurbita maxima*. *Planta* 109:193–210.
12. Sabnis DD, Hart JW (1973) P-protein in sieve elements. I. Ultrastructure after treatment with vinblastine and colchicine. *Planta* 109:127–133.
13. Behnke H-D, Schulz A (1980) Fine structure, pattern of division, and course of wound phloem in *Coleus blumei*. *Planta* 150:357–365.
14. Wu J-L, Hao B-Z (1990) Ultrastructure of P-protein in *Hevea brasiliensis* during sieve-tube development and after wounding. *Protoplasma* 153:186–192.
15. Read SM, Northcote DH (1983) Subunit structure and interactions of the phloem proteins of *Cucurbita maxima* (pumpkin). *Eur J Biochem* 134:561–569.
16. Furch ACU, Zimmermann MR, Will T, Hafke JB, van Bel AJE (2010) Remote-controlled stop of phloem mass flow by biphasic occlusion in *Cucurbita maxima*. *J Exp Bot* 61: 3697–3708.
17. Anderson R, Cronshaw J (1970) Sieve-plate pores in Tobacco and Bean. *Planta* 91: 173–180.

18. Beyenbach J, Weber C, Kleinig H (1974) Sieve-tube proteins from *Cucurbita maxima*. *Planta* 119:113–124.
19. Clark AM, et al. (1997) Molecular characterization of a phloem-specific gene encoding the filament protein, phloem protein 1 (PP1), from *Cucurbita maxima*. *Plant J* 12:49–61.
20. Golecki B, Schulz A, Thompson GA (1999) Translocation of structural P proteins in the phloem. *Plant Cell* 11:127–140.
21. Lin M-K, Lee Y-J, Lough TJ, Phinney BS, Lucas WJ (2009) Analysis of the pumpkin phloem proteome provides insights into angiosperm sieve tube function. *Mol Cell Proteomics* 8:343–356.
22. Zhang B, Tolstikov V, Turnbull C, Hicks LM, Fiehn O (2010) Divergent metabolome and proteome suggest functional independence of dual phloem transport systems in cucurbits. *Proc Natl Acad Sci USA* 107:13532–13537.
23. Noll GA (2005) Molekularbiologische Charakterisierung der Forisome. Dissertation (Justus-Liebig Universität, Gießen Germany).
24. Noll GA, et al. (2007) Spatial and temporal regulation of the forisome gene *for1* in the phloem during plant development. *Plant Mol Biol* 65:285–294.
25. Noll GA, et al. (2011) Characteristics of artificial forisomes from plants and yeast. *Bioeng Bugs* 2:111–114.
26. Pélissier HC, Peters WS, Collier R, van Bel AJE, Knoblauch M (2008) GFP tagging of sieve element occlusion (SEO) proteins results in green fluorescent forisomes. *Plant Cell Physiol* 49:1699–1710.
27. Müller B, et al. (2010) Recombinant artificial forisomes provide ample quantities of smart biomaterials for use in technical devices. *Appl Microbiol Biotechnol* 88:689–698.
28. Rüping B, et al. (2010) Molecular and phylogenetic characterization of the sieve element occlusion gene family in Fabaceae and non-Fabaceae plants. *BMC Plant Biol* 10:219.
29. Knoblauch M, Peters WS, Ehlers K, van Bel AJE (2001) Reversible calcium-regulated stopcocks in legume sieve tubes. *Plant Cell* 13:1221–1230.
30. Knoblauch M, et al. (2003) ATP-independent contractile proteins from plants. *Nat Mater* 2:600–603.
31. Noll GA, et al. (2009) The promoters of forisome genes *MtSEO2* and *MtSEO3* direct gene expression to immature sieve elements in *Medicago truncatula* and *Nicotiana tabacum*. *Plant Mol Biol Rep* 27:526–533.
32. Bucsenez M, et al. (2012) Multiple *cis*-regulatory elements are involved in the complex regulation of the sieve element-specific *MtSEO-F1* promoter from *Medicago truncatula*. *Plant Biol (Stuttg)*, 10.1111/j.1438-8677.2011.00556.x.
33. Sabnis DD, Sabnis HM (1995) *The Cambial Derivatives*, ed Iqbal M (Borntraeger, Berlin), pp 271–292.
34. Noll GA, et al. (2011) Native and artificial forisomes: Functions and applications. *Appl Microbiol Biotechnol* 89:1675–1682.
35. Ernst AM, et al. (2011) The *sieve element occlusion* gene family in dicotyledonous plants. *Plant Signal Behav* 6:151–153.
36. Turgeon R (1989) The sink-source transition in leaves. *Annu Rev Plant Physiol Plant Mol Biol* 40(1):119–138.
37. Evert RF (1977) Phloem structure and histochemistry. *Annu Rev Plant Physiol* 28(1): 199–222.
38. Imlau A, Truernit E, Sauer N (1999) Cell-to-cell and long-distance trafficking of the green fluorescent protein in the phloem and symplastic unloading of the protein into sink tissues. *Plant Cell* 11:309–322.
39. Voinnet O, Rivas S, Mestre P, Baulcombe D (2003) An enhanced transient expression system in plants based on suppression of gene silencing by the p19 protein of tomato bushy stunt virus. *Plant J* 33:949–956.
40. King RW, Zeevaart JAD (1974) Enhancement of Phloem exudation from cut petioles by chelating agents. *Plant Physiol* 53:96–103.
41. Costello LR, Bassham JA, Calvin M (1982) Enhancement of phloem exudation from *Fraxinus uhdei* Wenz. (Evergreen Ash) using ethylenediaminetetraacetic acid. *Plant Physiol* 69:77–82.
42. Evert RF, Derr WF (1964) Callose substance in sieve elements. *Am J Bot* 51:552–559.
43. van Bel AJE (2003) The phloem, a miracle of ingenuity. *Plant Cell Environ* 26:125–149.
44. Mullendore DL, Windt CW, Van As H, Knoblauch M (2010) Sieve tube geometry in relation to phloem flow. *Plant Cell* 22:579–593.
45. Batailler B, et al. (2012) Soluble and filamentous proteins in Arabidopsis sieve elements. *Plant Cell Environ* 35:1258–1273.
46. Sauer N (2007) Molecular physiology of higher plant sucrose transporters. *FEBS Lett* 581:2309–2317.
47. Ehlers K, Knoblauch M, van Bel AJE (2000) Ultrastructural features of well-preserved and injured sieve elements: Minute clamps keep the phloem transport conduits free for mass flow. *Protoplasma* 214:80–92.
48. Lee DR, Arnold DC, Fensom DS (1971) Some microscopical observations of functioning sieve tubes of *Heracleum* using Nomarski optics. *J Exp Bot* 22:25–38.
49. Hartig T (1854) Ueber die Querscheidewaende zwischen den einzelnen Gliedern der Siebröhren in *Cucurbita pepo*. *Botanische Zeitung* 12:51–54.
50. Froelich DR, et al. (2011) Phloem ultrastructure and pressure flow: Sieve-Element-Occlusion-Related agglomerations do not affect translocation. *Plant Cell* 23: 4428–4445.
51. Kleinig H, Thönes J, Dörr I, Kollmann R (1975) Filament formation *in vitro* of a sieve tube protein from *Cucurbita maxima* and *Cucurbita pepo*. *Planta* 127:163–170.
52. Eschrich W, Evert RF, Heyser W (1971) Proteins of the sieve-tube exudate of *Cucurbita maxima*. *Planta* 100:208–221.
53. Nuske J, Eschrich W (1976) Synthesis of P-protein in mature phloem of *Cucurbita maxima*. *Planta* 132:109–118.
54. Walker TS, Thaine R (1971) Proteins and fine structural components in exudate from sieve tubes in *Cucurbita pepo* stems. *Ann Bot (Lond)* 35:773–790.
55. Alosi MC, Melroy DL, Park RB (1988) The regulation of gelation of Phloem exudate from *cucurbita* fruit by dilution, glutathione, and glutathione reductase. *Plant Physiol* 86:1089–1094.
56. Schwan S, Fritzsche M, Cismak A, Heilmann A, Spohn U (2007) *In vitro* investigation of the geometric contraction behavior of chemo-mechanical P-protein aggregates (forisomes). *Biophys Chem* 125:444–452.
57. Knoblauch M, Peters WS (2004) Forisomes, a novel type of $Ca^{(2+)}$-dependent contractile protein motor. *Cell Motil Cytoskeleton* 58:137–142.
58. Wergin WP, Newcomb EH (1970) Formation and dispersal of crystalline P-Protein in sieve elements of soybean (*Glycine max* L.). *Protoplasma* 71:365–388.
59. Altschul SF, Gish W, Miller W, Myers EW, Lipman DJ (1990) Basic local alignment search tool. *J Mol Biol* 215:403–410.
60. Schmidt GW, Delaney SK (2010) Stable internal reference genes for normalization of real-time RT-PCR in tobacco (*Nicotiana tabacum*) during development and abiotic stress. *Mol Genet Genomics* 283:233–241.
61. Hoekema A, Hirsch PR, Hooykaas PJJ, Schilperoort RA (1983) A binary plant vector strategy based on separation of *vir*- and T-region of the *Agrobacterium tumefaciens* Ti-plasmid. *Nature* 303:179–180.
62. Horsch RB, et al. (1986) Analysis of Agrobacterium tumefaciens virulence mutants in leaf discs. *Proc Natl Acad Sci USA* 83:2571–2575.
63. Murashige T, Skoog F (1962) A revised medium for rapid growth and bioassays with tobacco tissue cultures. *Physiol Plant* 15:473–497.
64. Jefferson RA (1987) Assaying chimeric genes in plants: The GUS gene fusion system. *Plant Mol Biol Rep* 5:387–405.
65. Felts K, et al. (2000) Recombinant *Renilla reniformis* GFP displays low toxicity. *Strategies* 13(3):85–87.
66. Collier R, Fuchs B, Walter N, Kevin Lutke W, Taylor CG (2005) Ex vitro composite plants: An inexpensive, rapid method for root biology. *Plant J* 43:449–457.
67. Thompson MV, Wolniak SM (2008) A plasma membrane-anchored fluorescent protein fusion illuminates sieve element plasma membranes in Arabidopsis and tobacco. *Plant Physiol* 146:1599–1610.
68. Hawes C, Satiat-Jeunemaitre B (2001) *Plant cell biology: a practical approach*, eds Hawes C, Satiat-Jeunemaitre B (Oxford Univ Press, Oxford, UK), pp 235–266.
69. Moran DT, Rowley JC (1987) *Correlative Microscopy in Biology: Instrumentation and Methods*, ed Hayat MA (Academic, New York), pp 1–22.
70. Reynolds ES (1963) The use of lead citrate at high pH as an electron-opaque stain in electron microscopy. *J Cell Biol* 17:208–212.